REPORT SD-TR-89-64

(4)

Thermionic Emission Including Both Space Charge and Image Forces

T. P. LIN and G. ENG
Chemistry and Physics Laboratory
Laboratory Operations
The Aerospace Corporation
El Segundo, CA 90245-4691

1 September 1989

Prepared for

SPACE SYSTEMS DIVISION
AIR FORCE SYSTEMS COMMAND
Los Angeles Air Force Base
P.O. Box 92960
Los Angeles, CA 90009-2960

REPORT DOCUMENTATION PAGE

1a. REPORT SECURITY CLASSIFICATION Unclassified	1b. RESTRICTIVE MARKINGS
2a. SECURITY CLASSIFICATION AUTHORITY	3. DISTRIBUTION/AVAILABILITY OF REPORT Approved for public release; distribution unlimited.
2b. DECLASSIFICATION/DOWNGRADING SCHEDULE	
4. PERFORMING ORGANIZATION REPORT NUMBER(S) TR-0086A(2945-02)-2	5. MONITORING ORGANIZATION REPORT NUMBER(S)
6a. NAME OF PERFORMING ORGANIZATION The Aerospace Corporation Laboratory Operations 6b. OFFICE SYMBOL *(If applicable)*	7a. NAME OF MONITORING ORGANIZATION Space Systems Division
6c. ADDRESS *(City, State, and ZIP Code)* El Segundo, CA 90245	7b. ADDRESS *(City, State, and ZIP Code)* Los Angeles Air Force Base Los Angeles, CA 90009-2960
8a. NAME OF FUNDING/SPONSORING ORGANIZATION 8b. OFFICE SYMBOL *(If applicable)*	9. PROCUREMENT INSTRUMENT IDENTIFICATION NUMBER F04701-85-C-0086
8c. ADDRESS *(City, State, and ZIP Code)*	10. SOURCE OF FUNDING NUMBERS PROGRAM ELEMENT NO. / PROJECT NO. / TASK NO. / WORK UNIT ACCESSION NO.

11. TITLE *(Include Security Classification)*

Thermionic Emission Including Both Space Charge and Image Forces

12. PERSONAL AUTHOR(S)

Lin, T. P., and Eng, G.

13a. TYPE OF REPORT	13b. TIME COVERED FROM _____ TO _____	14. DATE OF REPORT *(Year, Month, Day)*	15. PAGE COUNT
			35

16. SUPPLEMENTARY NOTATION

17. COSATI CODES			18. SUBJECT TERMS *(Continue on reverse if necessary and identify by block number)*
FIELD	GROUP	SUB-GROUP	Thermionic Emission Cathodes Poisson's Equation

19. ABSTRACT *(Continue on reverse if necessary and identify by block number)*

The net emission current for a uniform planar thermionic emitter is determined for a range of voltages, temperatures, and various values of the work function. Poisson's equation is self-consistently solved, using numerical techniques, without any additional phenomenological assumptions. This work accurately specifies the net current in the transition region between space-charge-limited and temperature-limited emission, and we present the first determination of the shape of the interelectrode potential there. A comparison with earlier approximate techniques is also included.

20. DISTRIBUTION/AVAILABILITY OF ABSTRACT	21. ABSTRACT SECURITY CLASSIFICATION
☐ UNCLASSIFIED/UNLIMITED ☐ SAME AS RPT. ☐ DTIC USERS	Unclassified
22a. NAME OF RESPONSIBLE INDIVIDUAL	22b. TELEPHONE *(Include Area Code)* / 22c. OFFICE SYMBOL

PREFACE

The permanent address for Professor T. P. Lin is the Department of Mathematics, California State University, Northridge, Northridge, CA, 91330.

CONTENTS

I. INTRODUCTION

Most cathodes operate at a temperature high enough to begin life in the space-charge-limited (SCL) emission region. In that region, the net current is insensitive to small changes in cathode temperature and surface work function. However, during operation, the cathode work function often gradually increases, until the undesirable temperature-limited (TL) emission region is reached, often ending the cathode useful life. It is therefore important to understand not only the SCL and TL emission limits but also where the SCL-to-TL transition is, and how gradual it should be.

Previous theoretical treatments of electron emission have resulted in the well-known Child[1]-Langmuir[2] law for SCL emission, and the Richardson[3] equation with Schottky barrier lowering[4] for TL emission. Each law is a limiting case approximation and is not valid for the whole range. Nottingham[5] improved the Langmuir-Child formalism to aid its calculability. Van der Ziel,[6] Crowell,[7] and Rittner[8] made additional refinements, but they did not include the effect of Schottky barrier lowering in the TL region.

As far as we are aware, no previous treatment accurately covers the entire range, including the SCL-to-TL transition. Recently, there have been some efforts by Longo,[9] Scott,[10] Hasker,[11] and Eng[12] to combine the SCL and TL limits using various approximation techniques. However, it is difficult to quantitatively ascertain the effects of each approximation, a priori especially in the transition region.

In this work, we sought to unify the SCL and TL emission limits by solving the full Poisson's equation including both space-charge and image-force effects. Numerical techniques are used, without any additional simplifying assumptions.

Our results converge to the proper SCL and TL emission limits, as well as accurately specifying the net current in the transition region between SCL and TL emission. In addition, we present the first determination of the shape of the interelectrode potential in the transition region between SCL and TL emission. We then calculate the first principles of cathode current-voltage (I-V) and current-temperature (I-T) behavior.

II. POISSON'S EQUATION FOR ELECTRON EMISSION

Poisson's equation relates the electrostatic potential V to the local number density of electrons $\tilde{n}(x)$:

$$\nabla^2 V = e\tilde{n}(x)/\epsilon_o, \tag{1}$$

where ϵ_o is the permittivity of free space, and $e = +1.602 \times 10^{-19}$ coulombs. Poisson's equation assumes that electrostatics dominate the forces acting on an individual electron. It ignores explicit time-dependent (non-equilibrium) effects, and disregards the small magnetic field created by the presence of a moving electron current.

In the simplest case of planar geometry, there is enough symmetry in the boundary conditions so that only one spatial variable remains, and the Laplacian operator becomes:

$$\nabla^2 = \frac{d^2}{dx^2}. \tag{2}$$

Poisson's equation must then be solved, taking both electron energy conservation and current conservation into account.

A. SPACE-CHARGE EFFECTS

For planar geometry, the momentum component along the direction of electron flow varies with the potential field, but the momentum components in the other orthogonal directions remain constant. Hence we need to consider only the momentum p along the current flow direction. Energy conservation can be written as:

$$E = (p^2/2m) - eV = (p_c^2/2m) - eV_c \ , \tag{3}$$

where E is the electron total energy, [-eV] is the potential energy component, and V_c and p_c are the values for the potential and the electron momentum at the cathode.

The electron density due to space-charge effects, $\tilde{n}(x)$, can be derived from an electron distribution function $n(p,x)$ by:

$$\tilde{n}(x) = \int_{p_m(x)}^{\infty} n(p,x)\, dp = \int_{E_m(x)}^{\infty} \hat{n}(E,x)\, dE, \qquad (4)$$

where $n(p,x)$ is the fraction of electrons at x with momenta between p and $p+dp$. The value of the momentum p is taken to be positive in the direction of net current flow, and $p_m(x)$ is the minimum momentum that electrons can have at that position. In Eq. (4), $\hat{n}(E,x)$ is the fraction of electrons at x, sorted by energy instead of momentum, and $E_m(x)$ is the minimum total energy for electrons at that point.

Since both the total energy E and the net current density J_o are conserved quantities, the fractional amount of current density $dJ(E)$, comprised of electrons of energy between E and $E+dE$, is also conserved. Thus, $dJ(E)$ must be independent of the spatial variable x. The equation:

$$dJ(E) = \hat{n}(E,x)\, e\, v(E,x)\, dE\ , \qquad (5)$$

then relates changes in the local electron velocity $v(E,x)$ to changes in the local electron density $\hat{n}(E,x)$. Taken together, current conservation [Eq. (5)] and energy conservation [Eq. (3)] determine $n(p,x)$:

$$n(p,x) = (1/e)\, dJ(E)/dE\ , \qquad (6)$$

showing that $n(p,x)$ is also independent of position.

All surfaces have a work function Φ, which is an intrinsic barrier to spontaneous electron emission into the vacuum. For most solids, Φ = (1.5, 5.5) eV. When thermal energies are small compared with Φ, and given macroscopic applied fields, one can assume that the distribution of electrons just outside the cathode surface is Maxwellian:

$$n(p_c,x_c) = (J_o/ekT) \exp\,[-E/kT], \qquad (7)$$

where x_c is the position of the cathode surface. In Eq. (7), the E=0 point is chosen to be the top of the electrostatic energy barrier (see Fig. 1), J_o is the net emitted current density, T is in Kelvin, m is the electron mass, and k is Boltzmann's constant.

Substituting Eqs. (3) and (7) into Eq. (4) results in:

$$\tilde{n}(x) = (J_o/e)\ (\pi m/2kT)^{1/2}\ P(\psi), \tag{8a}$$

$$\psi = eV/kT, \tag{8b}$$

$$P(\psi) = (\exp\ \psi)\ \frac{2}{\pi^{1/2}}\ \int_{p_m(x)}^{\infty} \exp(-p^2/2mkT)\ dp/(2mkT)^{1/2}. \tag{8c}$$

Because ψ depends on V(x), the function $P(\psi)$ also implicitly depends on x, making Poisson's equation nonlinear.

The energy scale defined by Eq. (7) means that an electron with total energy E=0 barely surmounts the electrostatic barrier. For the region $x=(x_b,x_a)$, between the barrier maximum (x_b) and the anode or collector (x_a), all the electrons have a total energy E>0 and each contributes to the collected current. For the region $x=(x_c,x_b)$, between the cathode (x_c) and the barrier maximum, some electrons have a total energy E<0, and they will be turned back by the barrier. The minimum momentum in this region corresponds to the reflected electron with the highest energy. Both cases can be summarized together, resulting in the following expression for p_m:

$$p_m = f\ (2mkT\ \psi)^{1/2}, \tag{9a}$$

$$f = \begin{cases} +1 & \text{for } x = (x_b,x_a) \\ -1 & \text{for } x = (x_c,x_b) \end{cases} . \tag{9b}$$

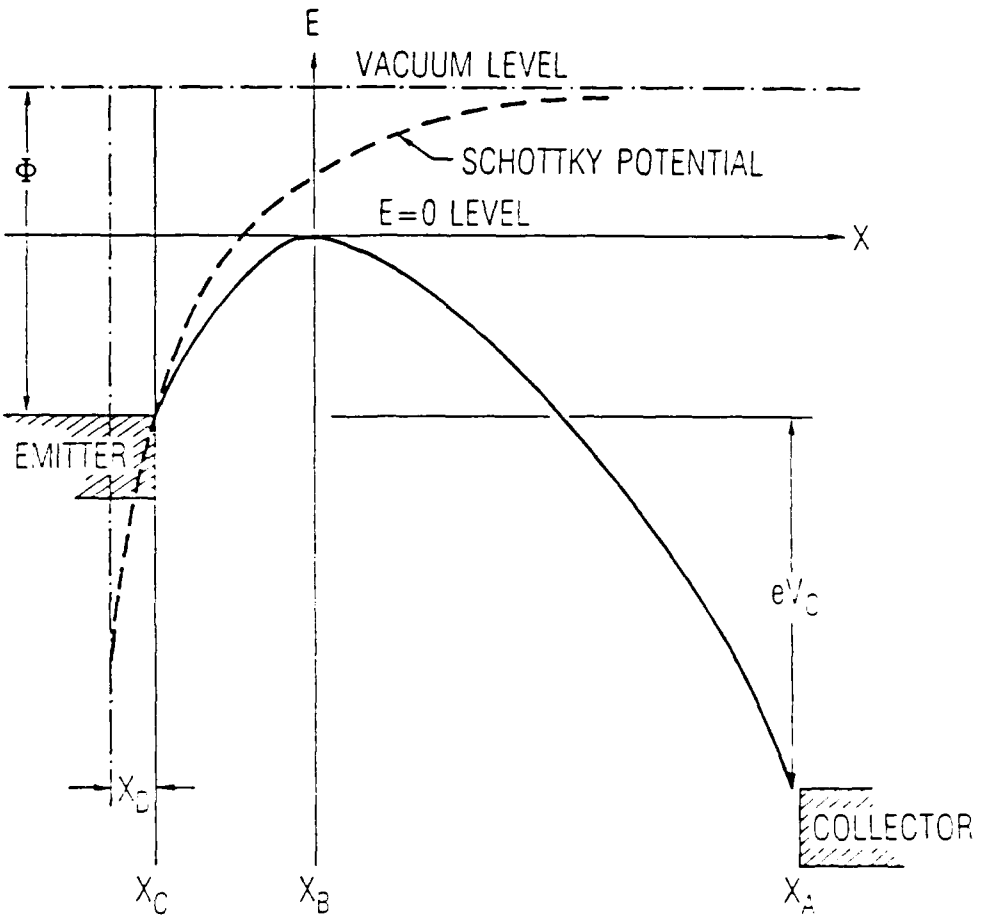

Figure 1: Schematic of the interelectrode potential energy. Space-charge effects cause an energy barrier to develop for emitted electrons, given an applied potential V_o. Also shown are the vacuum level and the Schottky potential due to image-force effects. The E=0 level here is chosen to be the barrier maximum at x_b, with the anode at x_a and the cathode at x_c. The work function determines x_d, the point at which the image force becomes singular.

B. IMAGE-FORCE EFFECTS

Up to this point, we have considered space-charge effects and have ignored the Schottky effect.[4] An electron placed in front of a conductor induces an opposite charge on the conductor, creating an attractive force equivalent to that exerted by a positron placed at:

$$x_p = 2(x_c - x_d) - x \ . \tag{10}$$

In Eq. (10), x_d offsets the mirror plane for the image charge so that it is slightly inside the cathode. The electrostatic force between the electron and its image is given by Coulomb's law:

$$\vec{F} = [-e^2/4\pi\varepsilon_o(x-x_p)^2]\ \vec{x}_o, \tag{11}$$

where $\vec{x}_o$ is a unit vector from the cathode to the collector.

A Schottky potential Q can be derived from $\vec{F}$ using:

$$\nabla\cdot\vec{F} = e\nabla^2 Q. \tag{12}$$

It shows that the image force contributes a singular term to the charge density in Poisson's equation:

$$\nabla^2 Q = d^2Q/dx^2 = 2e/[16\pi\varepsilon_o|x + x_d - x_c|^3]. \tag{13}$$

To determine the value of x_d, we note that the potential energy difference for a single electron at $x = x_c$, relative to the vacuum level, is exactly the cathode work function:

$$e\ Q(x_c) = \Phi, \tag{14}$$

n the absence of applied fields. The image force contribution [Eq. (13)], together with the space-charge terms [Eqs. (8a)-(8c)], makes Poisson's equation both nonlinear and inhomogeneous.

C. DIMENSIONLESS VARIABLES

The numerical computations can be simplified by using the following scaling constants:

$$V_L = kT/e = \text{characteristic thermal voltage}, \tag{15a}$$

$$p_L = (2mkT)^{1/2} = \text{characteristic thermal momentum}, \tag{15b}$$

$$x_L = \left(\frac{\varepsilon_o}{e\,J_o}\right)^{1/2} \left(\frac{2\,k^3T^3}{\pi\,m}\right)^{1/4} = \text{thermal distance}. \tag{15c}$$

Poisson's equation can then be written in terms of the following dimensionless variables:

$$\psi \equiv eV/\kappa T = V/V_L = \text{scaled potential}, \tag{16a}$$

$$\tilde{x} \equiv (x-x_b)/x_L = \text{scaled distance}, \tag{16b}$$

which shifts the x-axis so that the barrier maximum becomes the new origin.

The Schottky image-force term then introduces a second length scale which competes with the thermal length, x_L. It can be characterized by the following dimensionless constants:

$$\tilde{a} = (x_b + x_d - x_c)/x_L, \tag{17a}$$

$$\tilde{b} = \tilde{x}_s /x_L \tag{17b}$$

$$\tilde{x}_s = e^2/(16\,\pi\,\varepsilon_o kT). \tag{17c}$$

In terms of the dynamical variables, ψ and $\tilde{x}$, and the $\tilde{a}$ and $\tilde{b}$ constants, Poisson's equation becomes:

$$\frac{d^2\psi}{d\tilde{x}^2} = (1 - f)\exp(\psi^{1/2}) + f\,H(\psi^{1/2}) + 2\,\tilde{b}/|\tilde{x} + \tilde{a}|^3 \qquad (18a)$$

$$f = \begin{cases} +1 & \text{for } \tilde{x} = [0,\ (x_a - x_b)/x_L] \\ -1 & \text{for } \tilde{x} = [(x_c - x_b)/x_L,\ 0] \end{cases} \qquad (18b)$$

with the following boundary conditions:

$$\psi = 0 \text{ and } (d\psi/d\tilde{x}) = 0 \text{ at } \tilde{x} = 0. \qquad (19)$$

and where $H(z)$ is defined as:

$$H(z) = (\exp z^2)\,\frac{2}{\pi^{1/2}} \int_z^\infty \exp(-y^2)\,dy \qquad (20a)$$

$$= (\exp z^2)\,\mathrm{erfc}(z), \qquad z \geq 0, \qquad (20b)$$

III. SOLUTION OF POISSON'S EQUATION

A. METHOD OF SOLUTION

Equation (18a) is second order, inhomogeneous, and nonlinear, and it was solved numerically. The inputs to the computer program were the temperature T, cathode work function Φ, and the current density J_o. Richardson's equation,[3,14,15]

$$J_o = A_o T^2 \exp(\mu), \tag{21}$$

determines the scaled barrier height μ, with A_o=119.58 Amps/(cm^2-K^2) being Richardson's constant. From these inputs, a unique value for the scaled distance parameters, $\tilde{a}$ and $\tilde{b}$, can be self-consistently determined.

Poisson's equation was first solved numerically between x_b and x_c, using an initial guess for the value of $\tilde{a}$. The solution was then iterated until a value of $\tilde{a}$ was found where the scaled potential at the cathode surface $\tilde{s}$ matched the scaled barrier height μ. After an accurate value for $\tilde{a}$ was found, the potential V was determined from Eq. (18a), by a straightforward numerical computation.

B. CALCULATION RESULTS

Using the Poisson equation solution, we obtained the potential curves, barrier positions, and current-voltage characteristics under various conditions.

An example of the interelectrode potential energy function is shown in Fig. 2. The overall curvature between the anode and the cathode is due to space-charge effects. Inset(a)of Fig. 2 shows that the near cathode region has a very shallow barrier maximum 0.29 microns away from the cathode, indicating that the cathode is barely operating in SCL emission. Inset (b) shows the image force effects very near the cathode. The nearly flat slope in inset (b) means that the net emission is very close to the SCL-to-TL transition point.

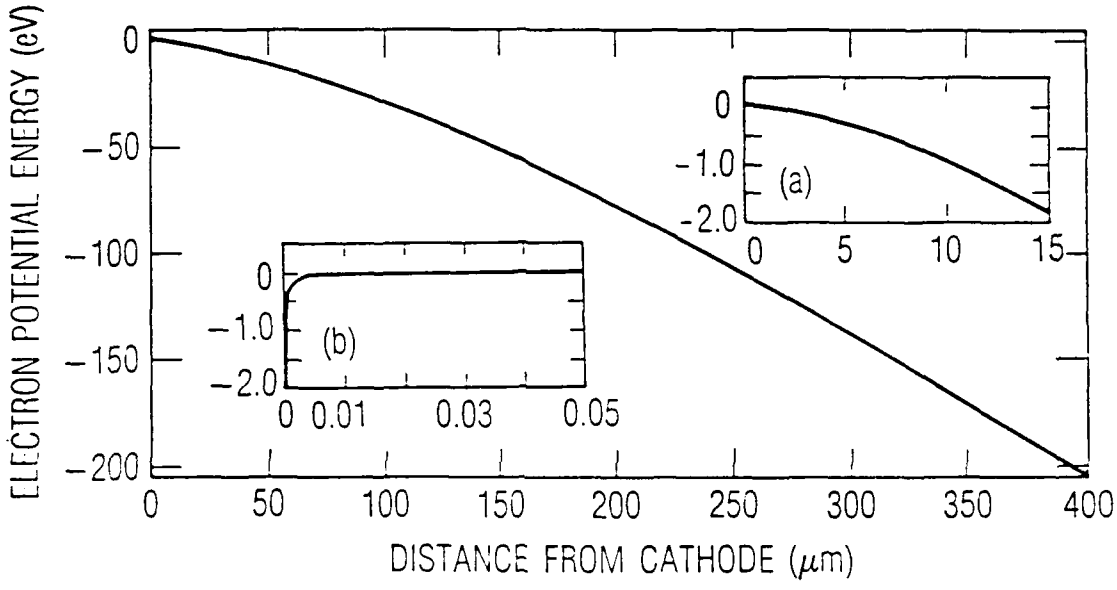

Figure 2: Sample calculation of the interelectrode potential energy near the SCL-to-TL transition. Space charge effects cause the observed curvature. Inset (a) has a barrier maximum 0.29 μm from the cathode. Inset (b) shows the very-near-cathode region where image-force effects are evident. Figs. 2-6 were done using a work function of 2.02 eV, and a 400 μm diode spacing. Here an applied voltage of 204 V and a temperature of 1050°C was also used, resulting in emission at 99.8% of the Richardson current value.

Figure 3 shows a set of calculated I-V curves for a uniform work function of 2.02 eV and temperatures between 925°C and 1150°C. At low voltages, the emission is nearly independent of temperature, consistent with the SCL emission law of Child and Langmuir. As the voltage increases, there is a sharp transition from SCL to TL emission (knee-region), but the knee becomes less sharp as the transition region moves to higher temperature or higher voltages.

For the SCL emission region, Child's law approximately relates the current density to the applied voltage V_o as:

$$J_o = K\, V_o^{3/2}, \tag{22}$$

where K is a constant. To compare our calculations with that law, we plotted the I-V curves on the log-log scale in Fig. 4. For most of the space-charge region, $J_o(V_o)$ has nearly a simple power dependence. However, the exponent value for V_o is closer to 1.4 rather than 3/2. The slight curvature in the log-log plot is due to the electron velocity distribution being taken into account and these results should be similar to the original Langmuir[2] extension of Child's law.

At the other extreme, for TL emission, the historical Schottky barrier lowering effect[4] is:

$$\mu = [\Phi - (e^3\, V_o/4\,\pi\,\varepsilon_o\, d_o)^{1/2}]/kT, \equiv [\Phi-\Delta\Phi]/kT, \tag{23}$$

where $d_o = |x_a - x_c|$ is the anode-cathode distance. Equation (23) has historically given rise to a method for estimating the cathode work function Φ. For a fixed electrode spacing and temperature, I-V data is plotted on $\log(J_o)$ vs. $V_o^{1/2}$ axes (Schottky plot). Using those axes, Eq. (23) should give a straight line in the high-voltage TL region. In this method, the work function Φ is then determined by extrapolating the straight line portion to V_o=0, and evaluating the intercept, where $\mu = \Phi/kT$.

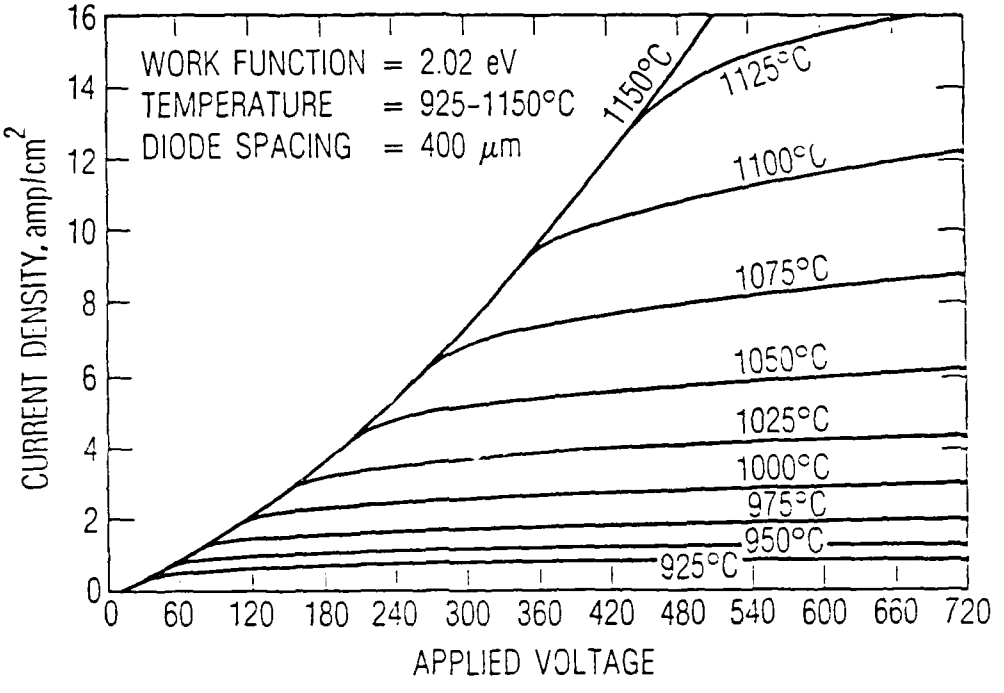

Figure 3: Calculated emission current density vs. voltage (I-V) curves for a temperature range of 925-1150°C. Each curve approaches the same function in SCL emission, followed by a sharp transition to TL emission behavior.

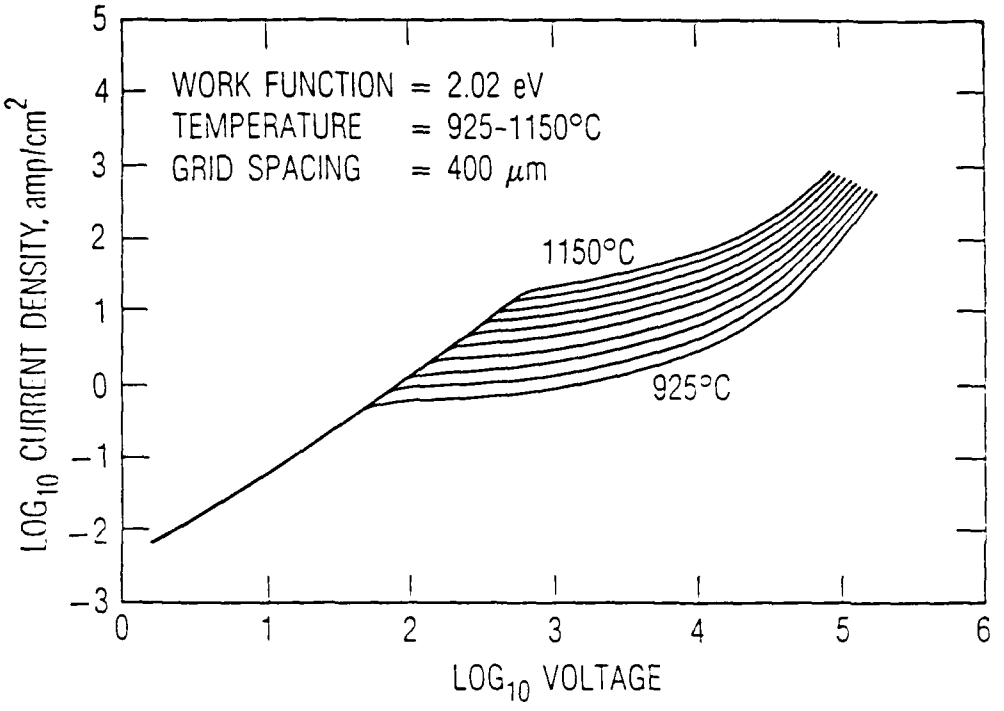

Figure 4: A log-log plot from the calculated I-V curves of Fig. 3. Child's Law gives a 3/2 slope. Our calculation shows a value closer to 1.4, with a slight curvature evident in the SCL region, due to the effects of a Maxwellian distribution for emitted electrons.

In Fig. 5, we show the results of a Schottky plot based on our I-V calculations. The calculated I-V values from the deep TL emission regime were then used to estimate the work function Φ from the Schottky plot. This Φ value was then compared against the input value that was initially used to generate the I-V curves. When we used very high voltages, for a wide range of temperatures and for work functions between 2.00-2.15 eV, we found that the deduced Φ differed from the input value by at most $\pm$ 0.002 eV. This result is a good indication of the internal consistency of our calculations.

The voltages used in this self-consistency check, however, are much higher than experimentally practicable (~ 20 KV on the scale of Fig. 5), thus Schottky plots cannot generally be used to estimate work function values from I-V data, as noted earlier by Hasker,[11] and by Eng,[12] who attributed this effect to the persistence of residual space-charge effects deep into the TL emission regime.

While the work function provides the most physical description of cathode activity, it is also difficult to measure, because I-V curves often require high applied voltages to drive the cathode into TL emission. Instead, one often relies on a current vs. temperature (I-T) test, because it can access the TL region without using high fields.

Typical results for the predicted I-T curves from this study are shown in Fig. 6. The high temperature portions of these curves are very nearly flat, indicating that the SCL emission current is practically temperature independent. The plot also determines how sharp the knee region between SCL and TL emission should be for a uniform work function surface. Figure 6 also shows that the transition region becomes more gradual at higher applied voltages, due to the increased net emission giving rise to a greater space-charge influence at the transition point.

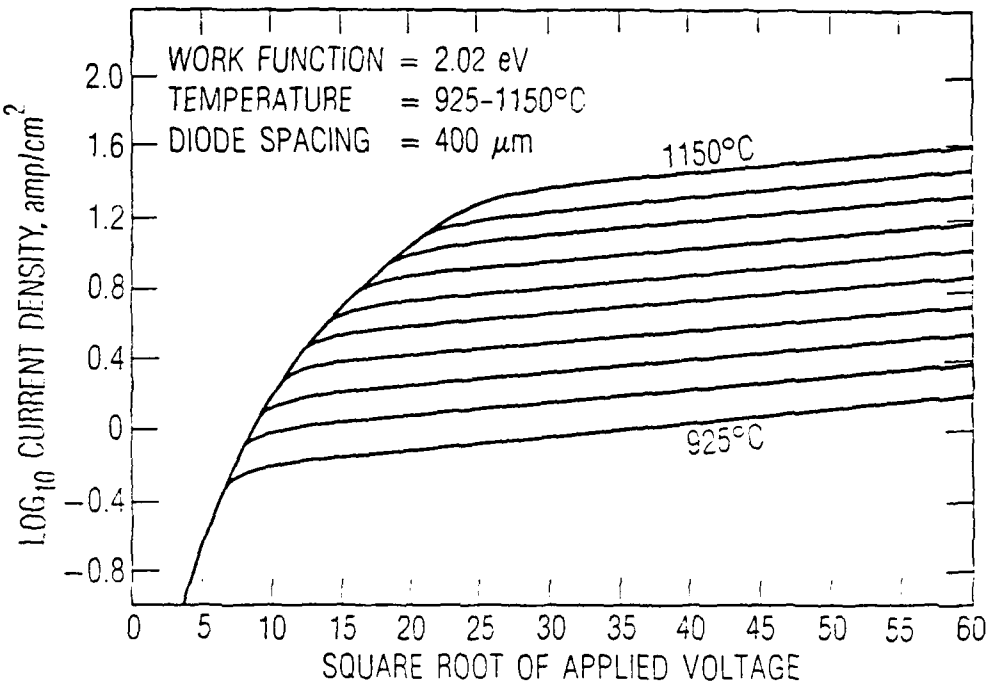

Figure 5: A Schottky plot from the I-V calculations, examining the deep TL emission region. Using these axes, the historical Schottky barrier lowering formula would result in a straight line. The work function derived by extrapolating the TL emission line from very high fields was found to agree to within ±0.002 eV of the input work function for values between 2.00 and 2.15 eV, showing the self-consistency of the calculation procedure.

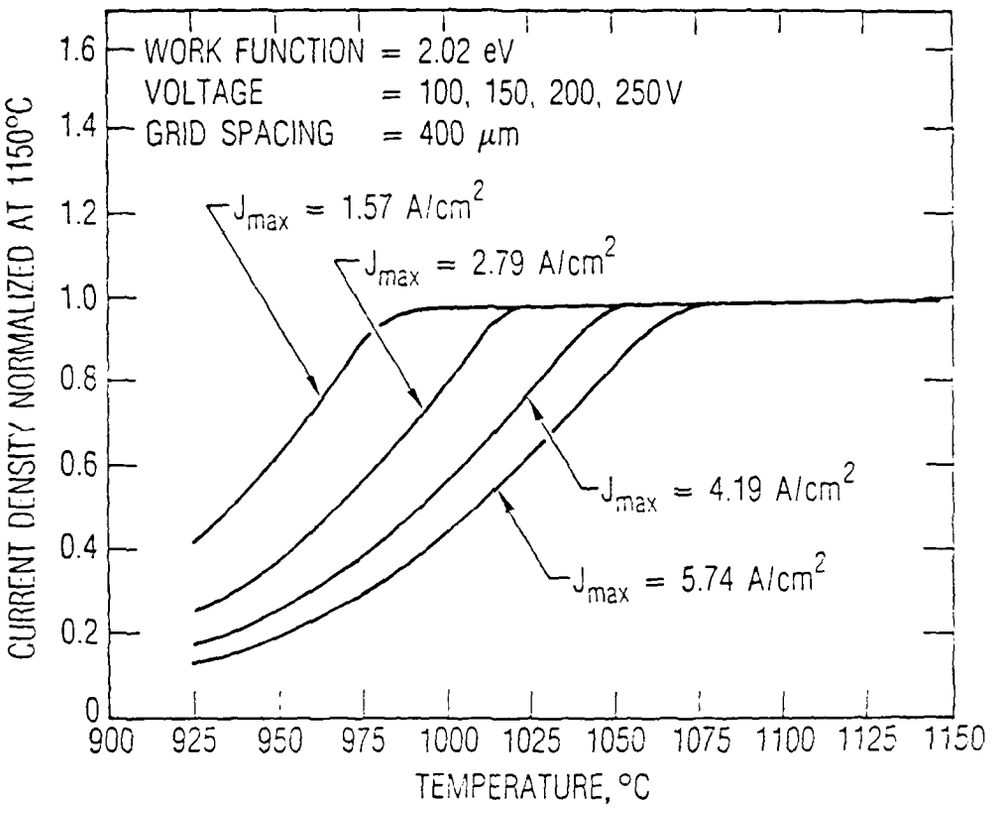

Figure 6: Calculated emission current vs. temperature (I-T) plots, normalized to unity at 1150°C, for a variety of applied voltages. Each voltage corresponds to different high temperature current density J_{max}. These curves also show that the SCL-TL transition region becomes more gradual at higher emission levels.

IV. COMPARISON WITH PRIOR APPROXIMATE METHODS

In this section, we compare the results of this first-principles numerical calculation of Poisson's equation containing both space-charge and image-force effects, to the earlier approximations of Longo,[9] Scott,[10] and Eng.[12]

Scott's method uses the Lagmuir[2] formalism for SCL emission, and he developed a way to extend that method into the TL regime by approximating the near-cathode field. Eng's analytic method approximated the inter-electrode potential for calculating the effects of space-charge. Longo's formula is semi-empirical and was based on cathode measurements.

In Fig. 7a, we compare the predicted I-V curves among these different methods, using logarithmic axes. It shows that both the Scott and Eng approximations are fairly accurate over a wide range of net currents. Those results are plotted using an expanded scale in Fig. 7b, to emphasize the SCL-to-TL transition region. It shows that the Scott method gives net emission currents which are a few percent high, while the Eng method gives values that are a few percent low.

In Fig. 8, the relative deviations among the various current predictions are shown. The Eng calculation was used as a 0% baseline because that method gives an I-V prediction which is both continuous, and has a continuous first derivative. The present results are also compared to the closed form approximation:[12]

$$J_{net} \cong J_R \exp\left[\frac{+\Delta\phi}{kT}\left(1 - \frac{J_{net}}{J_C}\right)^{1/2}\right] \quad (\text{for } J_R < J_C), \tag{24a}$$

$$J_{net} \cong J_C \ (\text{for } J_R \geq J_C), \tag{24b}$$

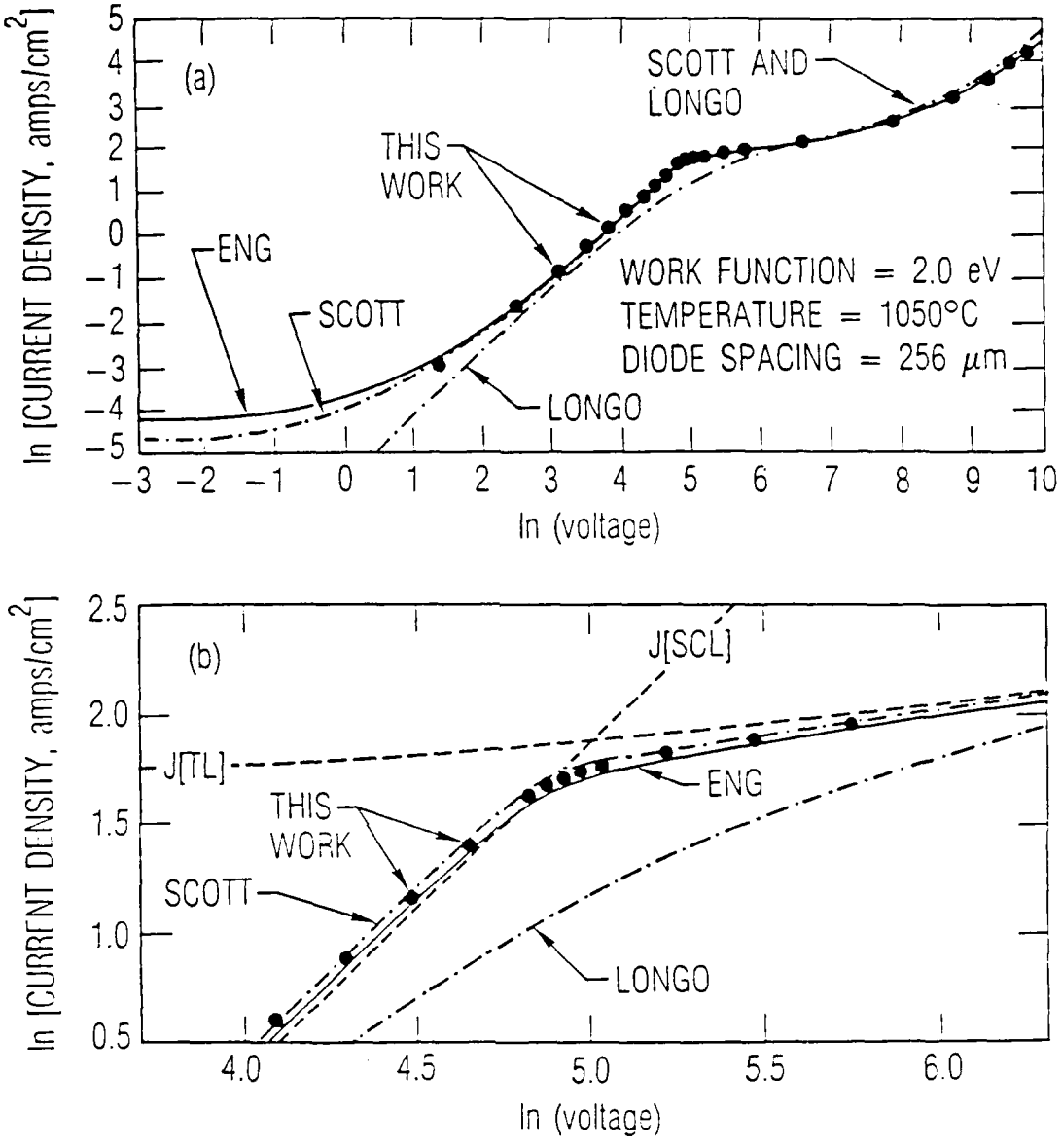

Figure 7: Current density vs. voltage predictions comparing this numerical method to the earlier approximate techniques of Longo, Scott, and Eng. Figs. 7-10 all use a 2.0 eV work function, a 256 μm anode-cathode spacing, and a 1050°C cathode temperature. On the large scale of Fig. 7a, both Scott's and Eng's calculations are similar to this work. In Fig. 7b, showing the SCL-to-TL transition, the Scott method predicts currents which are a few percent high, while the Eng method is a few percent low. Child's Law J[SCL], and the usual Schottky barrier-lowering current J[TL] are also shown.

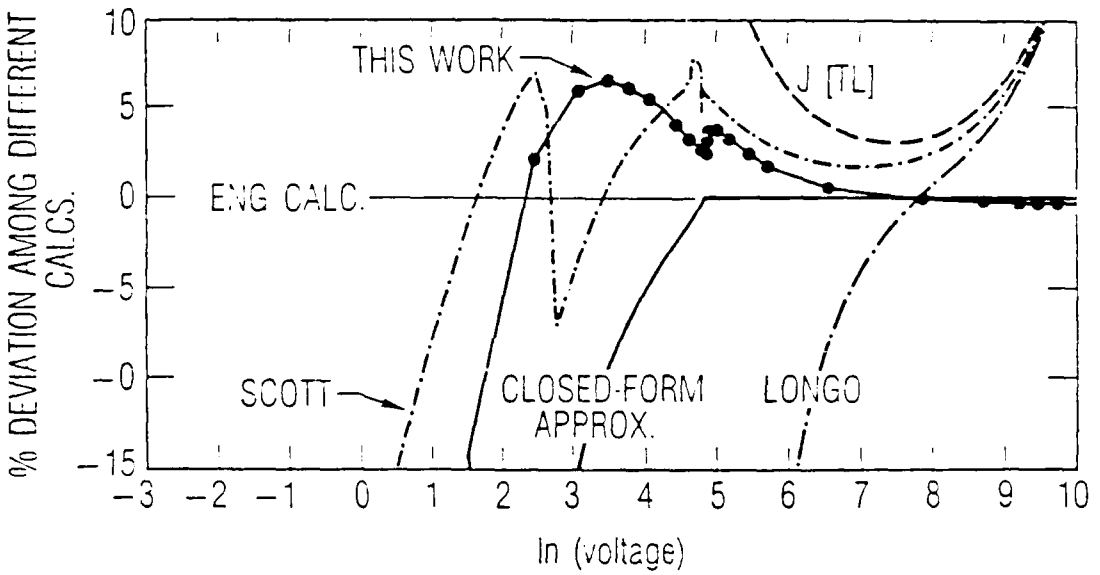

Figure 8: Comparison of the relative deviations among the different methods of net current computation. The earlier Eng work was used as a 0% baseline since that work was comprised of smooth analytic functions. Also shown is the accuracy of the closed-form approximation of Eq. (24).

where J_C and J_R are the usual Child's Law ($J_C \sim V^{3/2}$) and Richardson's currents, and where $+\Delta\phi$ is the usual Schottky barrier lowering from Eq. (23). Figure 8 clearly shows that the prior work of both Longo and Scott overestimates the TL current, while the above closed form developed by Eng is found to be quite accurate in that regime.

Both the earlier methods of Scott and Eng also give a prediction for the barrier position, and those are compared to the present calculation in Figs. 9a and 9b. The Scott method uses the Langmuir formalism for the SCL regime. In deep SCL emission, away from the transition region, the Langmuir formalism used by Scott (Fig. 9b) agrees almost identically with this first-principles calculation. A good agreement is expected here because image forces are not important in this regime. At these low voltages, the Eng method overestimates the barrier position by about a factor of 2, since it disregarded the effects of trapped near-cathode electrons.

Near the SCL-to-TL transition point, the present work and the Eng calculation give similar barrier position predictions, both having a steep change which marks the SCL-to-TL transition region. In contrast, the Scott method, which uses a Langmuir formalism for the SCL region, gives a barrier position that vanishes on the SCL side of the transition while subsequently predicting a barrier position infinitely far from the cathode on the TL side of the transition. This swing in the predicted barrier position from zero to infinity at the SCL-to-TL transition point in the Scott method explains why that method predicted I-V curves with a "kink" at this point.

Finally, in Figs. 10a and 10b, we show the asymptotic (near-anode) behavior of the interelectrode potential function covering both the SCL and TL emission regions. In Fig. 10a, each potential function was normalized to 100% being the net anode-to-cathode applied voltage, so as to emphasize the changes in the potential function shape.

The near-anode portion was then fit to the function $V(x) \sim x^p$ to examine how that exponent changes with applied field, and those results are shown in Fig. 10b. Child's Law predicts $p=4/3$ for SCL emission, while the

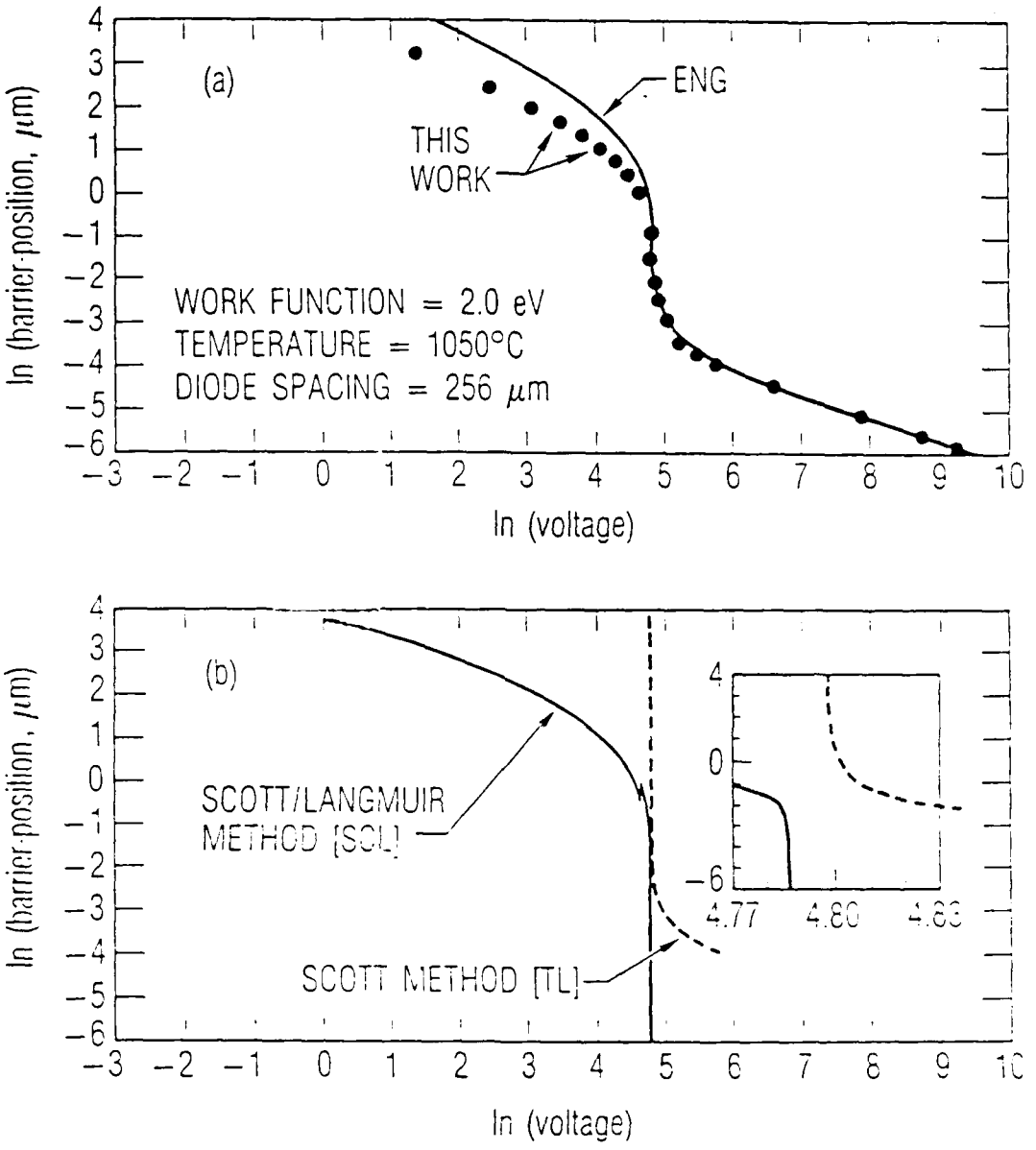

Figure 9: Barrier position as a function of voltage, with this numerical method compared to the earlier work of Scott and Eng. The Scott method is very inaccurate near the SCL-to-TL transition, where it gives a barrier position that varies from zero to infinity, as shown in the inset. The Eng method is quite accurate except in deep SCL emission, due to disregarding a trapped space-charge cloud near the cathode.

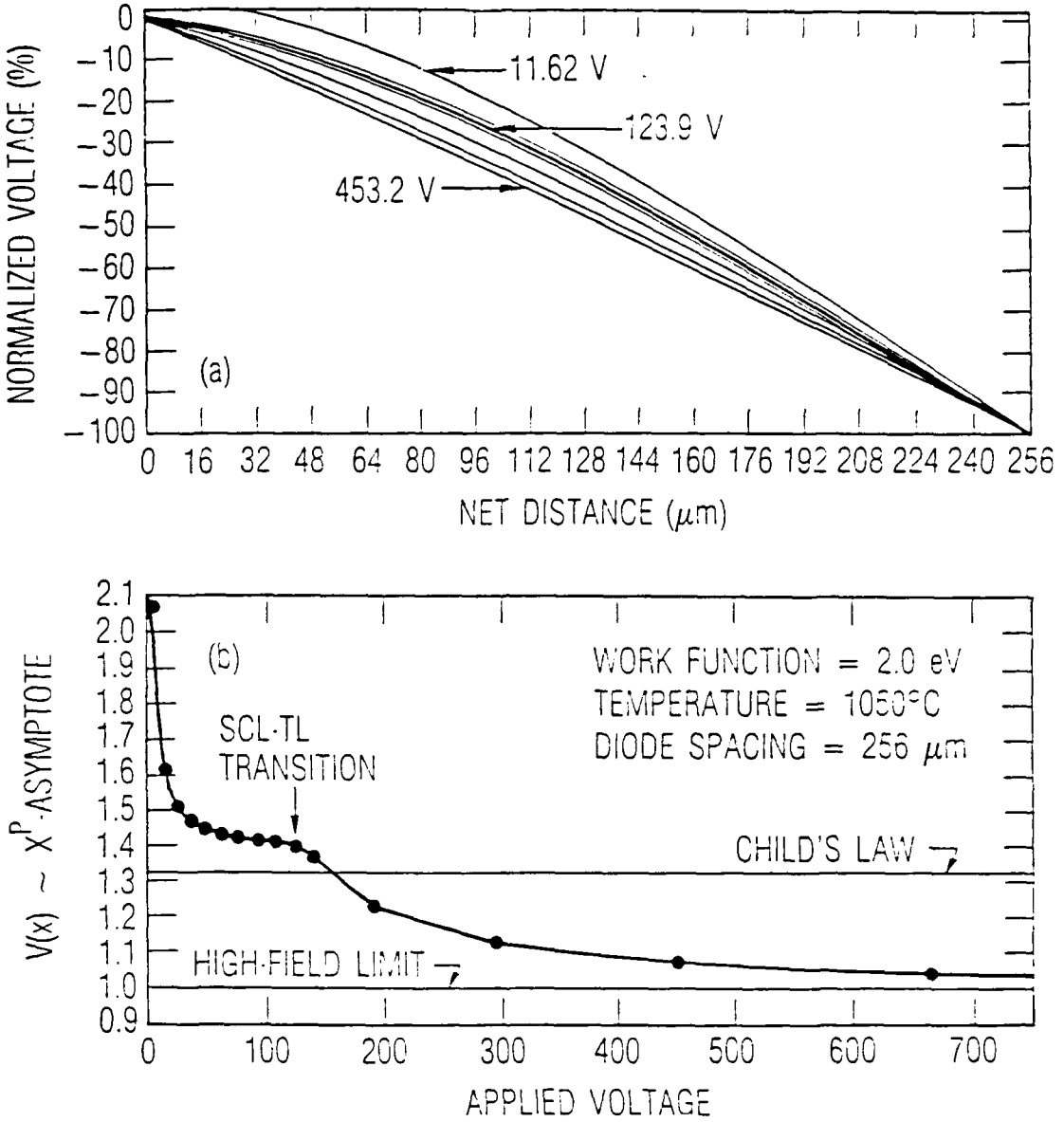

Figure 10: The interelectrode potential-energy function shape vs. applied voltage. Values used in Fig. 10a are: 11.62, 59.6, 123.9, 138.7, 190.8. 294.7, and 453.2 volts. Child's Law would have given a single universal curve with a power of p=4/3, while TL emission would be a linear function with power p=1. Fig. 10b shows how the power, p, actually changes with applied voltage, using this numerical calculation. The SCL-to-TL transition point is marked with an arrow.

historically-derived Schottky barrier lowering effect assumes p=1 for TL emission. However, the results of the present calculation show that a more complicated behavior is present.

At very low voltages, the interelectrode potential function is nearly parabolic ($p \tilde{=} 2$), corresponding to the charge density being nearly uniform throughout the anode-to-cathode region. As the applied voltage increases, a Child's Law type regime becomes evident, consistent with the space-charge cloud collapsing to become denser near the cathode. Here, we find the exponent is $p \tilde{=} 1.4$, instead of the Child's Law value 4/3, similar to the results shown in Fig. 4, where the SCL region behaves like $J \sim V^{1.4}$ instead of the Child's Law value of $J \sim V^{3/2}$.

The SCL-to-TL transition point is marked with an arrow on Fig. 10b, corresponding to where the barrier position changes most steeply. Beyond this point, the p-index then gradually approaches the p=1 value of TL emission. The gradual change in the p-value in the TL region, along with the demonstrated accuracy of Eqs. (24a) and (24b), further proves that space-charge effects persist well into the TL emission regime.

These results, taken together, show that both the recent approximate formalisms of Scott and Eng can be accurate to within a few percent for predicting net emitted current, while the Longo semi-empirical formula gives an I-V curve which changes too gradually to describe a uniform work-function surface. The barrier positions predicted by the Scott or Eng methods are also fairly good, except for the deep SCL regime in the Eng method, and the SCL-to-TL transition region for the Scott method.

Finally, the Eng closed-form approximation for unifying the SCL and TL emission limits [Eqs. (24a) and (24b)] is found to be very accurate above the SCL-to-TL transition point. Its accuracy in this regime, when compared to the numerical results, proves that the main ingredient required for unifying the Langmuir-Child and Schottky regimes is to take into account a space-charge correction to the normal Schottky barrier lowering effect.

V. CONCLUSIONS

A first-principles calculation for the electron emission from a uniform planar emitter was done using Poisson's equation and included both space-charge and image-force effects. The results were found to be consistent with the historically derived formulas for the SCL and TL emission limits, as well as smoothly bridging the transition region between them.

By providing the first direct calculation of the emission properties near the SCL-to-TL transition, we were able to show how sharp the knee region should be in a current vs. voltage or a current vs. temperature test for a uniform work function emitter. Also, by unifying the SCL and TL emission regimes through Poisson's equation, we were able to quantitatively predict how the shape of the interelectrode potential function changes, including in the critical SCL-to-TL transition regime, where all terms in the nonlinear Poisson's equation remain important.

The results of this numerical calculation were also compared to the prior approximate methods of Longo,[9] Scott,[10] and Eng.[12] The Longo formula has a SCL-to-TL transition which is much too gradual. The Scott method was found to be a few percent high in this regime, while the Eng method was a few percent low. In addition, the closed-form approximation [Eq. (24)] derived earlier by Eng was found to be very accurate for TL emission, showing that space-charge effects persist well into the classical temperature-limited emission regime.

REFERENCES

1. C. D. Child, Phy. Rev. 32, 498 (1911).
2. I. Langmuir, Phys. Rev. 21, 419 (1923).
3. O. W. Richardson, Phil. Mag. 23, 594 (1912)
4. W. Schottky, Z. Phys. 14, 63 (1923).
5. W. B. Nottingham, Handbuch der Physik, Vol. XXI, 1 (1960)
6. A. Van der Zeil, Philips Research Report, 1, 97, (1946).
7. C. R. Crowell, J. Appl. Phys. 26, 1353 (1955).
8. E. S. Rittner, J. Appl. Phys. 31, 1065 (1960).
9. R. T. Longo, 1980 Int'l. Electron Devices Meeting, Tech. Digest, 467-470 (1980).
10. J. B. Scott, J. Appl. Phys. 52, 4406 (1981).
11. J. Hasker, Appl. Surf. Sci. 16, 220 (1983).
12. G. Eng, J. Appl. Phys. 58, 4365 (1985).
13. C. Hastings, Jr., "Approximations for Digital Computers," Princeton Univ. Press, Princeton, N.J. (1955).
14. M. v. Laue, Jb. Radioakt. u. Elektr. 15, 205, 257, 301 (1918)
15. S. Dushman, Phys. Rev. 21, 623 (1923)

LABORATORY OPERATIONS

The Aerospace Corporation functions as an "architect-engineer" for national security projects, specializing in advanced military space systems. Providing research support, the corporation's Laboratory Operations conducts experimental and theoretical investigations that focus on the application of scientific and technical advances to such systems. Vital to the success of these investigations is the technical staff's wide-ranging expertise and its ability to stay current with new developments. This expertise is enhanced by a research program aimed at dealing with the many problems associated with rapidly evolving space systems. Contributing their capabilities to the research effort are these individual laboratories:

Aerophysics Laboratory: Launch vehicle and reentry fluid mechanics, heat transfer and flight dynamics; chemical and electric propulsion, propellant chemistry, chemical dynamics, environmental chemistry, trace detection; spacecraft structural mechanics, contamination, thermal and structural control; high temperature thermomechanics, gas kinetics and radiation; cw and pulsed chemical and excimer laser development including chemical kinetics, spectroscopy, optical resonators, beam control, atmospheric propagation, laser effects and countermeasures.

Chemistry and Physics Laboratory: Atmospheric chemical reactions, atmospheric optics, light scattering, state-specific chemical reactions and radiative signatures of missile plumes, sensor out-of-field-of-view rejection, applied laser spectroscopy, laser chemistry, laser optoelectronics, solar cell physics, battery electrochemistry, space vacuum and radiation effects on materials, lubrication and surface phenomena, thermionic emission, photosensitive materials and detectors, atomic frequency standards, and environmental chemistry.

Computer Science Laboratory: Program verification, program translation, performance-sensitive system design, distributed architectures for spaceborne computers, fault-tolerant computer systems, artificial intelligence, microelectronics applications, communication protocols, and computer security.

Electronics Research Laboratory: Microelectronics, solid-state device physics, compound semiconductors, radiation hardening; electro-optics, quantum electronics, solid-state lasers, optical propagation and communications; microwave semiconductor devices, microwave/millimeter wave measurements, diagnostics and radiometry, microwave/millimeter wave thermionic devices; atomic time and frequency standards; antennas, rf systems, electromagnetic propagation phenomena, space communication systems.

Materials Sciences Laboratory: Development of new materials: metals, alloys, ceramics, polymers and their composites, and new forms of carbon; nondestructive evaluation, component failure analysis and reliability; fracture mechanics and stress corrosion; analysis and evaluation of materials at cryogenic and elevated temperatures as well as in space and enemy-induced environments.

Space Sciences Laboratory: Magnetospheric, auroral and cosmic ray physics, wave-particle interactions, magnetospheric plasma waves; atmospheric and ionospheric physics, density and composition of the upper atmosphere, remote sensing using atmospheric radiation; solar physics, infrared astronomy, infrared signature analysis; effects of solar activity, magnetic storms and nuclear explosions on the earth's atmosphere, ionosphere and magnetosphere; effects of electromagnetic and particulate radiations on space systems; space instrumentation.